The Ox40/Ox40 Ligand Pathway Promotes Pathogenic Th Cell Responses, Plasmablast Accumulation, and Lupus Nephritis in NZB/W F1 Mice

Jonathan Sitrin,* Eric Suto,† Arthur Wuster,*,‡ Jeffrey Eastham-Anderson,§ Jeong M. Kim,¶ Cary D. Austin,§ Wyne P. Lee,† and Timothy W. Behrens*

Ox40 ligand (Ox40L) locus genetic variants are associated with the risk for systemic lupus erythematosus (SLE); however, it is unclear how Ox40L contributes to SLE pathogenesis. In this study, we evaluated the contribution of Ox40L and its cognate receptor, Ox40, using in vivo agonist and antagonist approaches in the NZB × NZW (NZB/W) F1 mouse model of SLE. Ox40 was highly expressed on several CD4 Th cell subsets in the spleen and kidney of diseased mice, and expression correlated with disease severity. Treatment of aged NZB/W F1 mice with agonist anti-Ox40 mAbs potently exacerbated renal disease, which was accompanied by activation of kidney-infiltrating T cells and cytokine production. The agonist mAbs also induced activation and inflammatory gene expression in splenic CD4 T cells, including IFN-regulated genes, increased the number of follicular helper T cells and plasmablasts in the spleen, and led to elevated levels of serum IgM and enhanced renal glomerular IgM deposition. In a type I IFN–accelerated lupus model, treatment with an antagonist Ox40:Fc fusion protein significantly delayed the onset of severe proteinuria and improved survival. These data support the hypothesis that the Ox40/Ox40L pathway drives cellular and humoral autoimmune responses during lupus nephritis in NZB/W F1 mice and emphasize the potential clinical value of targeting this pathway in human lupus. ***The Journal of Immunology*****, 2017, 199: 1238–1249.**

Systemic lupus erythematosus (SLE) is a multiorgan autoimmune disease characterized by aberrant cellular and humoral immune responses. Lupus nephritis (LN), one of the most common and severe clinical presentations of SLE, occurs in up to 50% of adults and 70% of children with the disease (1, 2). Despite decades of effort, most clinical trials for SLE have been disappointing, indicating the urgent need to identify and validate new therapeutic targets.

One key aspect of SLE pathophysiology is that immune complexes (ICs), consisting largely of autoantibodies, such as anti-dsDNA and anti-RNA–binding proteins, together with their cognate Ags, deposit in blood vessels and renal glomeruli, leading to vasculitis and nephritis [(3), reviewed in Refs. 4, 5)]. IC deposition results in the recruitment of lymphocytes and myeloid cells to kidney glomeruli, arterioles, and tubular interstitium, which further exacerbates renal damage.

Recent genome-wide association studies indicate that many immune-related pathways contribute to human SLE, and >50 genetic loci are now associated with disease risk (6). Understanding how these loci predispose to disease is critical for understanding disease etiology and for advancing therapeutic hypotheses. Ox40 ligand (Ox40L; *TNFSF4*) was originally identified as an SLE risk gene by Vyse and colleagues (7); however, only modest progress has been made in understanding its role in SLE pathogenesis.

Ox40L, and its cognate receptor, Ox40 (*TNFRSF4*), are members of the TNFR superfamily. There is significant evidence that this receptor/coreceptor pair is responsible for regulating adaptive T cell immune responses (reviewed in Refs. 8–11). In brief, Ox40L expression is largely restricted to APCs, whereas Ox40 is expressed primarily on activated or Ag-experienced Th cells and regulatory T cells (Tregs). Ox40 promotes Th cell survival (12–14), cytokine production (15), and memory cell formation and recall responses (16, 17). Ox40 may also have an important role in regulating the balance of effector T cell, Th cell, and Treg functions (18, 19).

Follicular helper T (Tfh) cells make up a specific helper cell subset that promotes humoral immune responses and has been implicated in lupus pathogenesis (20, 21). Tfh cells express Ox40, as well as other functional and identifying markers (e.g., CXCR5 and ICOS), and produce cytokines, such as IL-21. Disruption of

*Department of Human Genetics, Genentech, Inc., South San Francisco, CA 94080; †Department of Translational Immunology, Genentech, Inc., South San Francisco, CA 94080; ‡Department of Bioinformatics and Computational Biology, Genentech, Inc., South San Francisco, CA 94080; §Department of Pathology, Genentech, Inc., South San Francisco, CA 94080; and ¶Department of Cancer Immunology, Genentech, Inc., South San Francisco, CA 94080

ORCID: 0000-0002-5388-7413 (C.D.A.).

Received for publication April 27, 2017. Accepted for publication June 7, 2017.

This work was supported by Genentech, Inc.

J.S. conceptualized, designed, performed, and analyzed experiments and wrote the manuscript; E.S. designed and performed experiments; A.W. and J.E.-A. analyzed data; J.M.K. supervised and generated reagents; C.D.A. designed, performed, and analyzed experiments and edited the manuscript; W.P.L. supervised and designed experiments; and T.W.B. supervised and wrote and edited the manuscript.

The RNA sequencing data presented in this article have been submitted to the National Center for Biotechnology Information Gene Expression Omnibus (https://www.ncbi.nlm.nih.gov/geo/) under accession numbers GSE99645 and GSE99646.

Address correspondence and reprint requests to Dr. Jonathan Sitrin, Genentech, Inc., OMNI Human Genetics, 133003-4, MS93B, 1 DNA Way, South San Francisco, CA 94080. E-mail address: sitrinjr@gmail.com

The online version of this article contains supplemental material.

Abbreviations used in this article: cat. no., catalog number; GC, germinal center; IC, immune complex; IHC, immunohistochemistry; IPA, Ingenuity Pathway Analysis; LN, lupus nephritis; nRPKM, normalized read per kilobase gene model per million total reads; NZB/W, NZB × NZW; Ox40L, Ox40 ligand; PAS, periodic acid–Schiff; RNASeq, RNA sequencing; SLE, systemic lupus erythematosus; Tconv, Foxp3$^-$ conventional helper T; Tfh, follicular helper T; Treg, regulatory T cell.

Tfh cells or their key functional molecules ameliorate lupus symptoms in animal models (22). For example, in *Roquin*-deficient mice that develop lupus-like autoimmunity due to derepressed ICOS expression and Tfh cell activity (23), deletion of ICOS, SAP (a signaling molecule required for germinal centers [GCs]), or Bcl6 (a transcription factor required for Tfh cell development) disrupted Tfh cells and disease in these animals (24, 25). In addition to ICOS, Ox40 was recently found to be a direct target of the Roquin repressor protein family (26), highlighting the possibility that the Ox40 pathway might contribute to the disease phenotypes in those animals.

The specific function of Ox40 on Tfh cells is not entirely clear, in part due to conflicting results from various experimental models. Early work demonstrated a role for Ox40 in T-dependent anti-hapten IgG responses (27), but characterization of Ox40- and Ox40L-deficient animals found normal levels of Abs at rest, as well as in response to viral, hapten, or model Ag challenge (28–30). However, more recent studies targeting this pathway have identified defective GC and Ab responses in the context of Ox40 deficiency in response to viral infection (31, 32). Ox40 signaling leads to T cell accumulation in B cell follicles (33), increases the expression of CXCR5 (34–36), and enhances the production of cytokines, such as IFN-γ, IL-4, IL-6, and IL-10 (37, 38). Previous reports have also shown elevated Ox40 and Ox40L in SLE patient blood cells, serum, and kidney biopsies (reviewed in Ref. 11).

In the current study, we characterized the phenotype and function of Ox40-expressing cell populations during spontaneous disease in NZB × NZW (NZB/W) F1 lupus-prone mice. NZB/W F1 mice recapitulate several features of human SLE, including spontaneous onset, female-biased autoimmunity, and IC-mediated disease leading to nephritis and progressive renal failure (39). We assessed the effect of agonist anti-Ox40 mAbs and an antagonist Ox40:Fc fusion protein on disease features in NZB/W F1 mice. These data provide the first in vivo evidence, to our knowledge, that activation of Ox40 signaling promotes murine lupus pathogenesis and that blockade of this pathway may have disease-modifying activity.

Materials and Methods

Mice and disease monitoring

Female NZB/W F1 mice were bred and crossed at The Jackson Laboratory and then maintained at Genentech under specific pathogen–free conditions. All animal experimental protocols were approved by the Laboratory Animal Resources Committee at Genentech. For mouse lupus studies, renal disease severity was monitored by measuring proteinuria from fresh urine collected on a plastic sheet using Multistix 10 SG Reagent Strips and the CLINITEK Status Analyzer (both from Siemens). Animals were considered to have "severe" disease following multiple days of consecutive proteinuria readings ≥ 300 mg/dl.

In vivo treatments

An anti-Ox40 agonist mAb was generated by sequencing the rat anti-mouse Ox40 Ab (clone OX-86) and generating a chimeric fusion using the rat V region from OX-86 and a murine IgG1 Fc region. For anti-Ox40 agonist Ab treatments, cohorts were selected for age and proteinuria status at 12–13 wk (0 mg/dl proteinuria) or 21–27 wk (30–100 mg/dl proteinuria) and randomized by weight into treatment groups, and serum was collected prior to treatment for all experiments. Mice were treated s.c. with anti-Ox40 (IgG1) or an isotype-control IgG1 mAb (10 mg/kg three times per wk for 1–3 wk, depending on the experiment). During treatment and for the subsequent monitoring period, body weight and proteinuria were measured weekly, increasing to daily (if necessary) to monitor clinical symptoms. Animals were anesthetized under isoflurane and euthanized by terminal cardiac puncture or CO_2 inhalation.

The Ox40:Fc fusion protein construct was generated by fusing the extracellular domain (residues 20–198) of Tnfrsf4/Ox40 with a linker GVTGSGG to the N terminus (. . .CKPCIC. . .) of the H chain of murine IgG1 and by expressing the protein in CHO cells. Purification was performed using protein A affinity medium (MabSelect SuRe), followed by size exclusion chromatography (S200; both from GE Healthcare) to >95% purity by SDS–gel electrophoresis, <5% aggregate (analytical size-exclusion chromatography multi-angle static light scattering; Wyatt Technology), and <0.5 EU/mg. Functional binding of Ox40:Fc was confirmed using a cell line expressing murine Ox40L.

For IFN-α–accelerated lupus studies, mouse IFN-α5 was cloned into a pShuttleX vector and transferred into an Ad5 viral vector (Ad5–IFN-α) by the Baylor College of Medicine Vector Development Lab (Houston, TX). Twelve- to thirteen-week-old NZB/W F1 animals were randomized into treatment groups, and serum was collected prior to treatment. A single i.v. injection of the Ad5–IFN-α vector (1.2×10^8 PFU) was given 3 d prior to treatment with Ox40:Fc or a control Ig s.c. at a dose of 20 mg/kg, twice a week, for the duration of the experiment. Animals were monitored weekly for body weight and proteinuria, increasing to daily, if necessary. For survival studies, animals exhibiting severe moribund symptoms were euthanized. One animal from the control and Ox40:Fc treatment groups were removed from the analysis because they did not develop any symptoms of renal disease.

Serum collection, Ab titers, and autoantibody titers

Serum was collected via the tail vein or via retro-orbital bleeding under isoflurane anesthesia (for live animal experiments) or via cardiac puncture under isoflurane anesthesia (for terminal experiments). Serum was collected following clotting and column separation using Microvette 200 Z-Gel serum separators (order number 20.1291; Sarstedt), per the manufacturer's instructions. For experiments using anti-Ox40 agonist mAb treatment, serum was collected when animals exhibited proteinuria ≥ 300 mg/dl or at the end of the 3–4-wk experiment. Frozen serum was assayed using mouse anti-dsDNA IgG (catalog number [cat. no.] 5120), anti-ssDNA IgM (cat. no. 5330), anti-dsDNA IgM (cat. no. 5130), and anti–nuclear Ags Total Ig (cat. no. 5210) ELISA kits (Alpha Diagnostic International), per the manufacturer's instructions. Total Ab titers were measured by Luminex using the MILLIPLEX MAP Mouse Immunoglobulin Isotyping Magnetic Bead Panel (cat. no. MGAMMAG-300K; Millipore), per the manufacturer's instructions.

In vitro cultures

Splenic CD4 T cells were isolated from 21–27-wk-old (30–100 mg/dl proteinuria) NZB/W F1 mice using an EasySep Mouse CD4+ T Cell Isolation Kit (cat. no. 19852; STEMCELL Technologies), per the manufacturer's instructions, and cultured in a sterile round-bottom 96-well culture dish (cat. no. 3799; Costar), at 2.5×10^5 cells per well, with 10 U/ml IL-2 (product number 354043; Corning). Cells were treated with anti-Ox40 (IgG1) or an isotype-control IgG1 (25 μg/ml) along with a 0, 1:10, or 1:1 ratio of T cell activator (anti-CD3/CD28) Dynabeads (cat. no. 11452D; Thermo Fisher). After 48 h, conditioned media were collected, and cytokine titers were measured by Luminex using a MILLIPLEX MAP Mouse TH17 Magnetic Bead Panel (cat. no. MTH17MAG-47K) or a MILLIPLEX MAP Mouse Immunoglobulin Cytokine/Chemokine Magnetic Bead Panel (cat. no. MCYTMAG-70K-PX32; both from Millipore), per the manufacturer's instructions. Cellular RNA was collected for RNA sequencing (RNASeq).

Tissue histology

Tissues were harvested into 10% neutral buffered formalin fixative at room temperature, followed by embedding in paraffin for sectioning. Formalin-fixed paraffin-embedded 4-μm histologic kidney sections were stained with periodic acid–Schiff (PAS) for visual evaluation of glomerulonephritis or with H&E for visual evaluation of interstitial inflammation by light microscopy.

Glomerulonephritis severity scoring used a four-point semiquantitative scale: 0, normal or mild global lesions in <50% of glomeruli; 1, global lesions in >50% of glomeruli, <20% of which are severe (defined as more than one segment with less than three patent capillaries); 2, global lesions in >50% of glomeruli, 20–80% of which are severe; and 3, >80% of glomeruli with severe global lesions. Interstitial inflammation was similarly scored based on three separate parameters: tubulointerstitial nephritis (0, normal; 1, mild or focal inflammation not expanding the tubulointerstitium; 2, occasional moderately sized inflammatory infiltrates expanding the tubulointerstitium; and 3, frequent large-sized inflammatory infiltrates expanding the tubulointerstitium), periarteritis (0, normal; 1, sparse or focal moderate-sized inflammatory infiltrates; 2, occasional moderate-sized inflammatory infiltrates, generally not circumferential; and 3, frequent large inflammatory infiltrates, often circumferential), and pyelitis (0, normal; 1, sparse or focal moderate-sized inflammatory infiltrates; 2, occasional moderate-sized inflammatory infiltrates, not expanding the pelvic submucosa; and 3, frequent large inflammatory infiltrates, expanding the

pelvic submucosa). A glomerular cellularity score was obtained from PAS/hematoxylin-stained slides using semiautomated digital image analysis after whole-slide scanning on an NanoZoomer HT (Olympus) as follows: 20 random glomeruli per animal were manually traced, and nuclei within each were counted automatically in MATLAB (MathWorks) using color and size criteria for nuclear recognition.

Immunohistochemistry and immunofluorescence

To assess renal T cell infiltration, immunohistochemistry (IHC) using rabbit anti-CD3 (SP7; cat. no. RM-9107-S; Thermo Scientific) was performed on formalin-fixed paraffin-embedded 3-μm kidney sections pretreated with Target Retrieval Solution (DAKO) for Ag retrieval. Naive rabbit clone DA1E (product number 3900S; Cell Signaling Technology) and naive rat IgG2b (A95-1; cat. no. 553986; BD Pharmingen) were used in parallel as nonspecific isotype controls. Detection used goat anti-rabbit biotinylated IgG or rabbit anti-rat biotinylated IgG (both from Vector Laboratories), followed by VECTASTAIN Elite ABC peroxidase (Vector Laboratories) and DAB visualization (Thermo Fisher Scientific). Images were captured on a Leica DM6000 B microscope using a Leica DFC500 camera and Leica Application Suite software (Leica Microsystems, Wetzlar, Germany). To compare renal CD3 T cell frequency in anti-Ox40–treated and control Ig–treated mice, one slide from each treatment group was randomly paired with the other and visually compared in a blinded fashion: the slide with relatively more frequent T cells was assigned a score of 1, and the slide with relatively less frequent T cells was assigned a score of −1 (a score of 0 was assigned when both slides had comparable CD3 T cell frequency). Scoring of tubulointerstitial and glomerular T cell frequencies was performed separately.

Glomerular IC deposits were visualized on 5-μm acetone-fixed OCT-embedded kidney sections by direct immunofluorescence staining using Alexa Fluor 488–conjugated donkey anti-mouse IgG (cat. no. A-21202; Invitrogen), goat anti-mouse IgM (cat. no. A-21042; Invitrogen), or fluorescein-conjugated goat anti-complement C3 (cat. no. 55510; MP Biomedicals). Naive donkey or goat IgG (Jackson ImmunoResearch) was used in parallel as nonspecific isotype controls and were negative. Stained slides were scanned on a NanoZoomer XR (Hamamatsu), and morphologically intact renal cortex regions on each slide were manually selected and analyzed in MATLAB (MathWorks) to determine average pixel intensity in the selected area. A threshold filter was used to eliminate nonspecific background and enrich for glomerular signal, and a normalization factor was applied to combine two independent replicate cohorts.

GCs were visualized on 5-μm paraformaldehyde-fixed OCT-embedded spleen sections by indirect immunofluorescence staining after Ag retrieval with DAKO Target Retrieval Solution (code S1700), using the B cell and T cell activation and GC marker, GL7 (cat. no. 14-5902; eBioscience) and detected with Biotin Mouse Anti-Rat IgM (clone G53-238; cat. no. 550330; BD Pharmingen), followed by Alexa Fluor 546–conjugated streptavidin (cat. no. S11225; Molecular Probes, Thermo Fisher Scientific). GCs were visualized on an epifluorescence-equipped Leica DM6000 B microscope and imaged with a Leica DFC500 camera and Leica Application Suite software. GCs were manually counted on each spleen section, as clusters of at least five adjacent $GL7^+$ cells, in a blinded fashion.

Flow cytometry and cell sorting

Postmortem intracardial perfusion was performed with 20 ml of PBS. Spleen and kidney were harvested, and tissues were harvested into RPMI 1640 media and weighed, followed by mechanical disruption with scissors into 1-mm pieces. Tissues were shaken at 37°C in digestion buffer (67 μg/ml Liberase DL [05466202001], 20 μg/ml DNase I [1010459001], 5% FBS [SKU number 2442; all from Sigma-Aldrich] in RPMI 1640) for 15 min. Samples were passed through a 40-μm filter (cat. no. 352340; Corning) into RPMI 1640 supplemented with 5% FBS and 2 mM EDTA. Cells were treated with ACK lysing buffer for 5 min on ice and blocked using FcR Blocking Reagent (order number 130-092-575; Miltenyi Biotec) before surface staining. Cells were independently FcR blocked before intracellular stains following fixation and permeabilization, using a Foxp3/Transcription Factor Staining Buffer Set (cat. no. 00-5523-00; eBioscience), per the manufacturer's instructions. mAbs used for staining cells in these experiments included CD45 (clone 30F-11; cat. no. 553080; BD), CD4 (RM4-5; cat. no. 560782; BD), CD19 (6D5; cat. no. 115534; BioLegend), CD3 (17A2, cat. no. 100214; BioLegend or cat. no. 56-032; eBioscience), CD44 (IM7; cat. no. 17-0441; eBioscience or cat. no. 560567; BD), CD62L (MEL-14; cat. no. 56-0621; eBioscience or cat. no. 104432; BioLegend), Ox40 (Ox-86; cat. no. 12-1341; eBioscience), Rat IgG1 kappa Isotype Control (eBRG1; cat. no. 12-4301; eBioscience), Ox40 (Ox-86; cat. no. 119410; BioLegend), Foxp3 (FJK-16s; cat. no. 17-5773; eBioscience), CD25 (PC61.5; cat. no. 12-0251-82; eBioscience), CXCR5 (2G8; cat. no. 551960; BD), Rat IgG2a Isotype Control (R35-95; cat. no. 553928; BD), Brilliant Violet 421 Streptavidin (cat. no. 405226; BioLegend), ICOS (15F9; cat. no. 46-9940; eBioscience), Hamster IgG Isotype Control (cat. no. 46-4914; eBioscience), Ki-67 (SolA15; cat. no. 14-5698-80; eBioscience), Rat IgG2a kappa Isotype Control (eBR2a, cat. no. 14-4321; eBioscience), CD21 (7E9; cat. no. 123412; BioLegend), CD23 (B3B4; cat. no. 563200; BD), IgM (RMM-1; cat. no. 406505; BioLegend), IgD (11.26c.2a; cat. no. 405716; BioLegend), CD138 (281-2; cat. no. 142507; BioLegend), and GL7 (cat. no. 144607; BioLegend). Dead cells were discriminated using the LIVE/DEAD Fixable Near-IR Dead Cell Stain Kit (cat. no. L10119; Thermo Fisher). Flow cytometry was performed using an LSR II (BD), and data were analyzed using FlowJo (TreeStar) software. For sorting and RNASeq experiments, cells were prepared as described above, with the exception of the prestain enrichment steps. Kidney tissues were cleaned and enriched for lymphocytes using a 40/60% Percoll gradient (SKU number P4937; Sigma-Aldrich) procedure, per the manufacturer's instructions. Spleen tissue was enriched for CD4 T cells using a Mouse CD4+ T Cell Isolation Kit (cat. no. 19852; STEMCELL Technologies), per the manufacturer's instructions. Following staining, cell sorting was performed on a FACSAria II (BD).

RNASeq and pathway analysis

For in vivo treatment experiments, live $CD45^+CD19^-CD3^+CD4^+$ T cells were sorted to high purity from the spleen ($n = 4$) and kidney ($n = 5$) after 1 wk (day 8) of anti-Ox40 agonist mAb treatment, followed by lysing with RLT buffer supplemented with 2-ME (Sigma-Aldrich). RNA was extracted using an RNeasy Mini Kit (cat. no. 74104) or an RNeasy Micro Kit (cat. no. 74004; both from QIAGEN), depending on input. For kidney samples, an RNeasy MinElute Cleanup Kit (cat. no. 74204; QIAGEN) was used. For all RNASeq experiments, a Nanodrop 8000 (Thermo Scientific) was used to quantify RNA, and integrity was measured using the Bioanalyzer RNA 6000 Pico Kit (Agilent). Libraries were prepared using the TruSeq RNA Library Prep Kit v2 (Illumina) with 100–500 ng of input and amplified using 10 cycles of PCR. Libraries were multiplexed and sequenced on a HiSeq 2500 System (Illumina), resulting in 15–26 million single-end 50 bp reads per library. Alignment, feature counting, normalization, and differential expression analysis were performed similar to as described previously (40), with few differences, which are listed below. In brief, HTSeqGenie (41) was used to perform filtering, alignment to GRCm38, and feature counting. Normalized reads per kilobase gene model per million total reads (nRPKM) values were computed as a measure of gene expression. Pairwise differential expression analysis was performed using voom and limma (42). For organ-specific differential gene-expression analysis, significant genes were filtered and identified as $p < 0.05$, nRPKM > 2, and fold change > 2 or < 0.5. For the four-way comparison, significant genes were filtered and identified by the same threshold settings but were included if they were significant in at least one organ. Pathway analysis was performed with Ingenuity Pathway Analysis (IPA) software (QIAGEN) using the Molecular and Cellular Functions module. Heat map euclidean clustering of genes was performed by plotting log 2–transformed fold change values for each replicate sample and each gene (log 2 floor set at −3 for all heat maps). Colored boxes indicate the degree of fold change (unique to each graph). Venn diagrams were generated at bioinformatics.psb.ugent.be/webtools/Venn/. IFN-α–responsive genes (>2 fold change) from splenic CD4 T cells were described previously (43). For the cytokine analysis, genes were included in the heatmap when they reached the following criteria: $p < 0.05$, nRPKM >2, and fold change >1.5 in at least one organ, for all genes with the cytokine classification by IPA. RNASeq data are available from the National Center for Biotechnology Information Gene Expression Omnibus (https://www.ncbi.nlm.nih.gov/geo/) under accession numbers GSE99645 and GSE99646.

Graphing and statistics

Data visualization and statistical analyses were performed with GraphPad Prism (GraphPad). For all in vivo cellular and Luminex experiments, p values were calculated using the Mann–Whitney U test. For in vitro culture cytokine RNA experiments ($n = 3$), a two-tailed unpaired t test was used. For renal disease survival (Kaplan–Meier) graphs, p values were calculated with the log-rank (Mantel-Cox) test, and hazard ratios were calculated using the log-rank test. For ordinal histology scoring experiments, p values were calculated using the χ^2 test. The p values were considered significant at $^*p < 0.05$, $^{**}p < 0.01$, $^{***}p < 0.001$, and $^{****}p < 0.0001$.

Results

Ox40-expressing CD4$^+$ T cells in the spleen and kidney of NZB/W F1 mice

Using flow cytometry of single-cell suspensions of spleen and kidney from NZB/W F1 mice over a range of disease severities (21–51 wk old), we found that Ox40 was highly expressed on CD4 T cells in both tissues (Fig. 1A) and was not detectable on other lymphoid or myeloid cells (data not shown). Ox40 was upregulated on CD4 T cells prior to the onset of proteinuria, and the frequency and number of these cells correlated with disease severity in both tissues (Fig. 1B).

Ox40$^+$ T cells were enriched for the proliferation marker Ki67, and most cells expressed the CD44$^+$CD62L$^-$ activated/memory cell phenotype (Supplemental Fig. 1A, 1B). Ox40$^+$ CD4 T cells were also enriched for Foxp3, a marker for Tregs (Fig. 1C), and CXCR5 and ICOS, markers for Tfh cells (Fig. 1D) (20, 21, 44). Foxp3$^-$ conventional helper T (Tconv) cells were also identified in the spleen and kidney (Fig. 1C, Supplemental Fig. 1C).

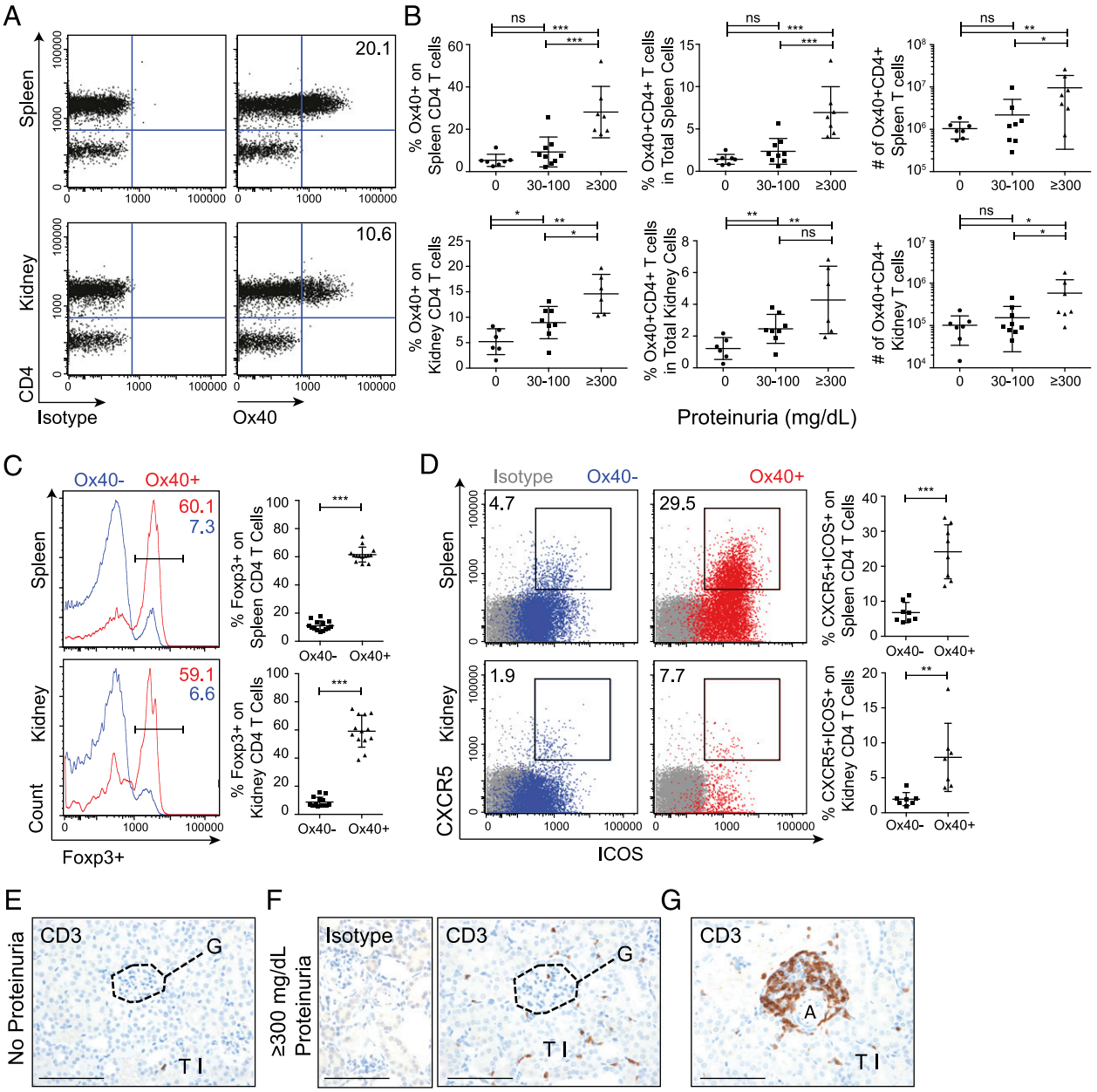

FIGURE 1. Ox40 expression on splenic and kidney-infiltrating CD4 T cell subsets in NZB/W F1 mice. (**A**–**D**) Spleen cells (top row) and kidney cells (bottom row) from NZB/W F1 mice (21–51 wk old). (A) Representative flow cytometry plots stained for an isotype control (left panels) or Ox40 (right panels) in gated live CD45$^+$CD19$^-$CD3$^+$ T cells. (B) Summary data from at least four independent experiments (mean ± SD) for the fraction of CD4 T cells expressing Ox40 (left panels), as well as the fraction (middle panels) and total number (right panels) of Ox40$^+$ CD4 T cells in total lymphocytes. (C and D) Representative flow cytometry plots and summary data from at least four independent experiments (mean ± SD). (C) Ox40$^-$ and Ox40$^+$ cells (gated on live CD19$^-$CD3$^+$CD4$^+$ T cells) intracellularly stained for Foxp3 and overlaid. (D) Gated live CD3$^+$CD4$^+$ T cells for Ox40$^-$ (left panels) and Ox40$^+$ (right panels) cells stained for CXCR5 and ICOS overlaid on top of isotype control (gray). (**E**–**G**) Representative fixed and CD3-stained kidney sections from NZB/W F1 mice from at least two independent experiments. Glomerular sections from proteinuria-free mice (E) and mice with proteinuria ≥300 mg/dl (isotype control stain, left panel) (F). (G) Periarterial and tubulointerstitial infiltrate from mice with ≥300 mg/dl proteinuria. Scale bars, 100 μm. *$p < 0.05$, **$p < 0.01$, ***$p < 0.001$. A, artery; G, glomerulus; TI, tubulointerstitium.

By IHC, $CD3^+$ kidney T cells were infrequent in NZB/W F1 mice prior to the onset of proteinuria (Fig. 1E), but they increased in abundance in diseased mice with ≥300 mg/dl proteinuria. T cells were found within or near renal glomeruli (Fig. 1F), in periarterial infiltrates, and throughout the tubulointerstitium (Fig. 1G).

Ox40 agonist mAbs exacerbate renal disease of aged NZB/W F1 mice

We next generated a novel anti-Ox40 agonist mouse IgG1 mAb (see *Materials and Methods*) and used it to determine the effect of Ox40 receptor stimulation in vivo in NZB/W F1 mice. Treatment of young mice (13 wk old, prior to the onset of proteinuria) with a 3-wk course (three injections per week) of anti-Ox40 agonist mAbs had no effect on the development of proteinuria compared with control Ig treatment (Fig. 2A). In contrast, renal disease was strongly exacerbated (reaching ≥300 mg/dl proteinuria) in three independent older cohorts with mild-to-moderate underlying disease (21–27 wk old, 30–100 mg/dl proteinuria, $n = 47$ animals in total) treated with the same regimen (Fig. 2B). A total of 89% of older mice treated with anti-Ox40 mAbs developed severe renal disease (median time to ≥300 mg/dl proteinuria = 14 d) compared with 51% in the control group (median time to ≥300 mg/dl proteinuria = 56 d, $p < 0.0001$) over the 84-d observation period.

Examination of fixed kidney sections harvested following anti-Ox40 mAb treatment showed increased severity of proliferative glomerulonephritis (Fig. 2C) and a corresponding increase in glomerular cellularity (Supplemental Fig. 1D) compared with control Ig treatment. Worse periarteritis and tubulointerstitial nephritis were also noted. From these data, we conclude that in vivo stimulation of Ox40 rapidly and efficiently exacerbated the onset of severe proteinuria and kidney disease in older NZB/W F1 mice. However, the same treatment had no effect on younger animals prior to the onset of proteinuria, despite those animals harboring Ox40-expressing cells (Fig. 1B).

Anti-Ox40 mAbs induce kidney IgM deposition and T cell activation

We next used immunofluorescent staining of frozen kidney sections to determine glomerular deposition of Igs and C3 following anti-Ox40 agonist mAb treatment. Staining was quantified using whole-slide scanning and digital image analysis (see *Materials and Methods*).

As expected, IgG deposition and IgM deposition in kidney renal cortex were increased during spontaneous progressive disease in control animals (Supplemental Fig. 1E). Of interest, we observed a significant increase in IgM deposits following

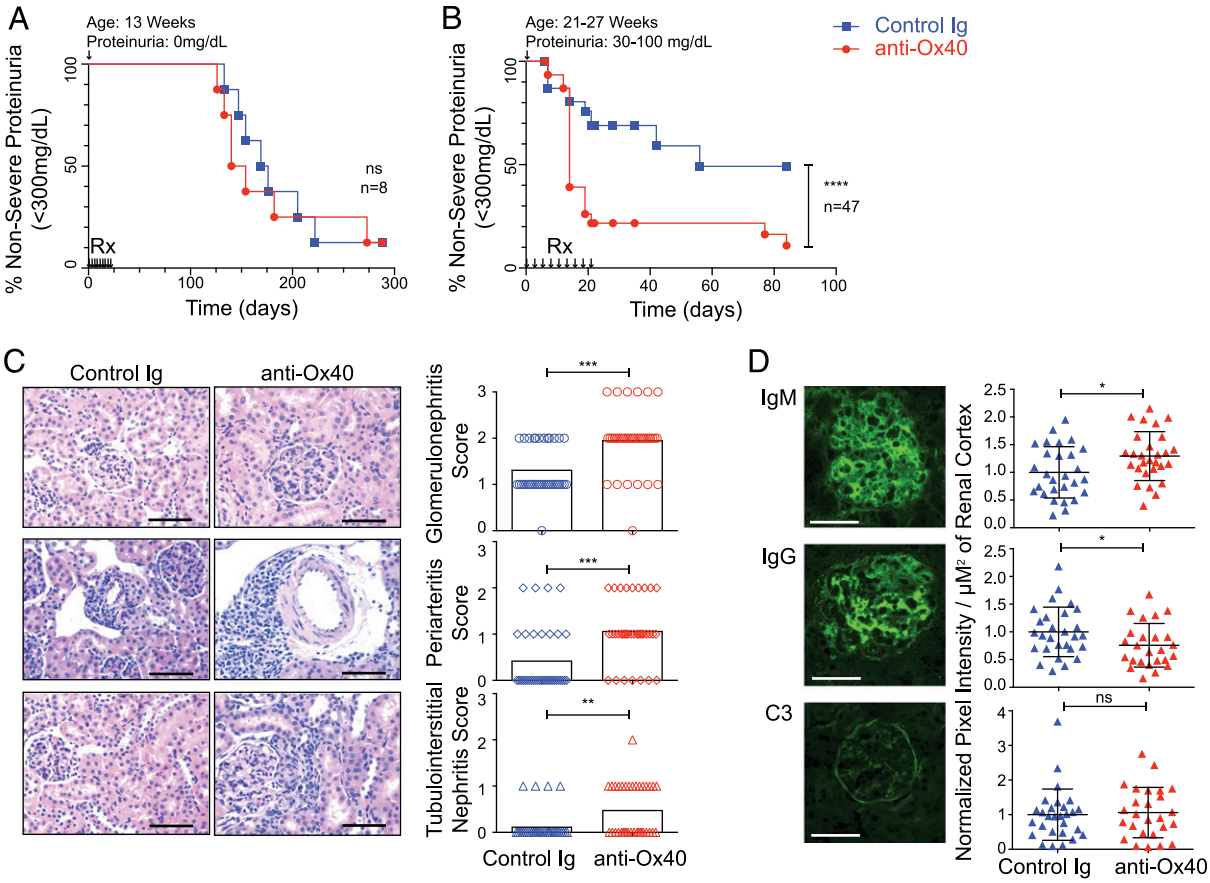

FIGURE 2. Anti-Ox40 agonist mAb treatment exacerbates renal disease and IgM deposition in NZB/W F1 mice. Renal disease monitoring following anti-Ox40 agonist mAb (red) and a control Ig (blue) treatment (10 mg/kg, three times per week for 3 wk) in NZB/W F1 mice. Black arrows (Rx) refer to treatment days. The age and proteinuria status of each cohort (at the time of first treatment) is indicated at the top of each plot. (**A**) Thirteen-week-old proteinuria-free NZB/W F1 mice at treatment start. (**B**) Three independent cohorts (21-, 26-, and 27-wk-old) of NZB/W F1 mice with proteinuria 30–100 mg/dl at treatment start. (**C**) Representative H&E- and PAS-stained kidney sections (left and middle panels) highlighting glomeruli (top panels), periarterial regions (middle panels), and tubulointerstitium (bottom panels). Scale bars, 100 μm. Corresponding disease severity scores (right panels). Group means are plotted in black ($n = 36$ per group combined). (**D**) Representative images from frozen kidney sections (left panels) stained for glomerular deposits of IgM (top panel), IgG (middle panel), and C3 (bottom panel). Scale bars, 50 μm. Corresponding signal intensity in the cortex regions is presented as pixel intensity/μM^2 of cortex with group mean ± SD from two independent cohorts ($n = 25$–28 per group, combined) (right panels). *$p < 0.05$, **$p < 0.01$, ***$p < 0.001$, ****$p < 0.0001$.

anti-Ox40 agonist mAb treatment compared with controls, whereas IgG deposition decreased, and C3 remained unchanged (Fig. 2D).

Following 1.5–3 wk of anti-Ox40 mAb treatment, there were no significant changes in kidney mass or infiltrating immune cell numbers, including total CD4 T cells (Supplemental Fig. 1F–J). A mild decrease in the percentage and number of $CD4^+Foxp3^-$ Tconv cells (Fig. 3A) and a small increase in the frequency of $CD4^+Foxp3^+$ Tregs (Supplemental Fig. 1K) were identified.

Despite the drop in cell numbers, Tconv cells were enriched for an activated/memory ($CD44^+CD62L^-$) phenotype following treatment (Fig. 3B). Using CD3 IHC staining on fixed kidney sections, we identified a significant increase in the relative frequency of glomerular and tubulointerstitial T cells following treatment (Fig. 3C, 3D).

Elevated serum IgM, splenic Tfh cells, and plasmablasts in Ox40 agonist mAb–treated mice

We next measured serum Ab levels and found a 45% elevation in total serum IgM in the anti-Ox40 mAb–treated group (Fig. 4A), consistent with the Ab deposit data in glomeruli (Fig. 2D). In contrast, serum IgG isotypes were decreased following treatment (Fig. 4B). Autoantibodies to dsDNA, ssDNA, and other nuclear Ags were not significantly affected (Supplemental Fig. 2A–E). Taken together, the observed increase in IgM and decrease in IgG deposition in glomeruli following anti-Ox40 mAb treatment were mirrored in the serum.

Examination of spleens after 1.5–3 wk of treatment showed no large changes in T cell numbers, but there was a slight increase in CD4 T cell frequency that was due, in part, to an expansion of $Foxp3^+$ Tregs (Supplemental Fig. 3A–F). Similar to the kidney T cell response, Tconv cells were enriched for an activated/memory phenotype ($CD44^+CD62L^-$) following treatment (Fig. 4C). Notably, we also observed an increase in $CXCR5^+ICOS^+$ Tfh cells (Fig. 4D).

B cell subsets were largely unaffected (Supplemental Fig. 3G–I). However, $CD138^+$ plasmablasts roughly doubled in number following anti-Ox40 agonist mAb treatment, including cells expressing IgM (Fig. 4E, 4F). Examination of spleens after 3 wk of treatment showed no increase in the number of GCs or GC phenotype cells, as measured by staining frozen spleen sections or live cell preparations for GL7 (Supplemental Fig. 2F, 2G).

T cell gene expression following Ox40 agonist mAb treatment in vivo

To better understand the molecular response of T cells following Ox40 receptor stimulation in vivo and to gain insight into potential mechanisms driving Ox40-exacerbated renal disease, we performed RNASeq on sorted CD4 T cells from the spleen and kidney following 1 wk of anti-Ox40 agonist mAb treatment.

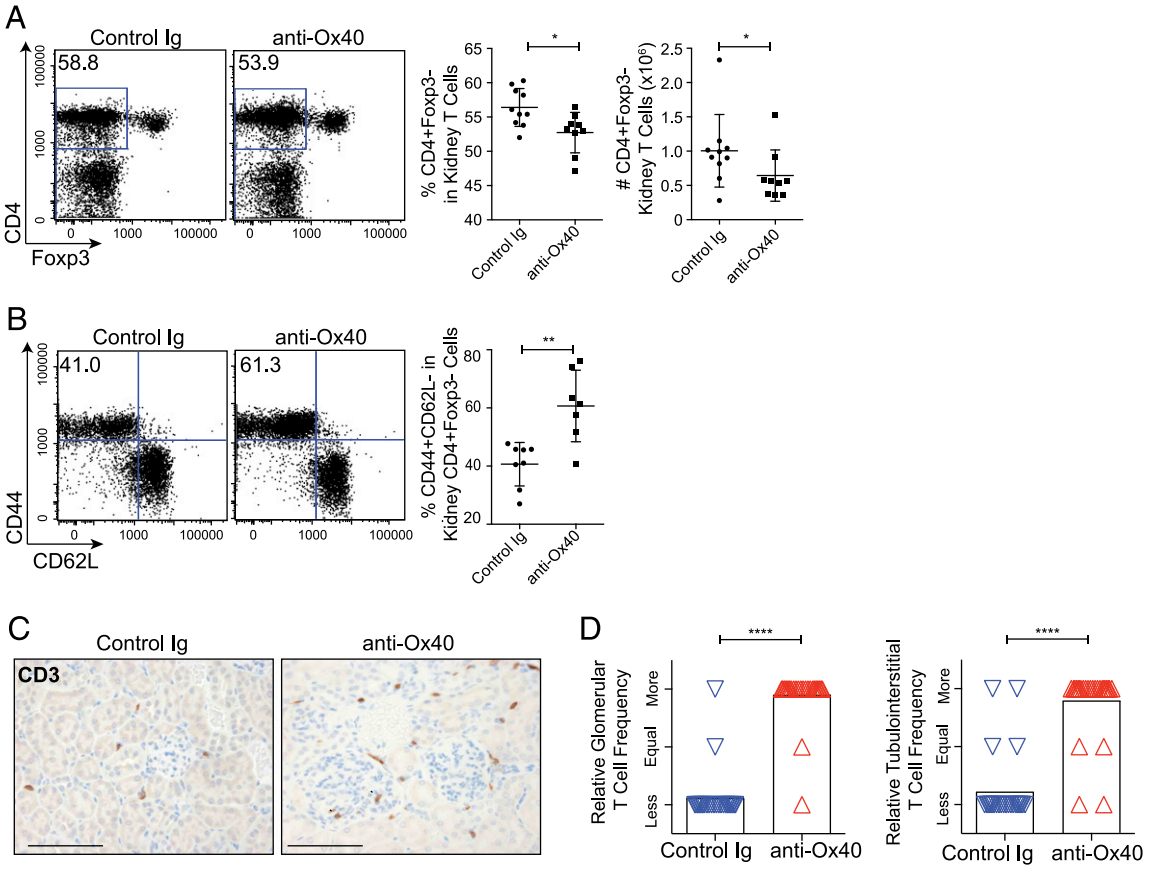

FIGURE 3. Ox40-stimulated kidney T cell response. (**A** and **B**) Representative flow cytometry plots (left panels) and summary data (right panels) from NZB/W F1 mice (21–27 wk old, 30–100 mg/dl proteinuria at treatment start) kidney cell preparations presented with mean ± SD from at least three independent experiments. (A) Frequency and number of Tconv cells (gated live $CD45^+CD3^+CD4^+Foxp3^-$). (B) Frequency of the activation/memory cell markers CD44 and CD62L on Tconv cells. (**C**) Representative images of kidney sections stained for $CD3^+$ T cells. Scale bars, 100 μm. (**D**) Blinded random-paired scoring of relative T cell frequency in control Ig–treated versus anti-Ox40 mAb–treated animals for glomerular cells (left panel) or tubulointerstitial cells (right panel). Scoring was based on a combination of two independent cohorts (n = 28 per group, combined). Small numbers (one to four) of infiltrating glomerular T cells were observed in a minority (~20%) of glomeruli and scattered within the interstitium, most often in the anti-Ox40 mAb–treated groups. *$p < 0.05$, **$p < 0.01$, ****$p < 0.0001$.

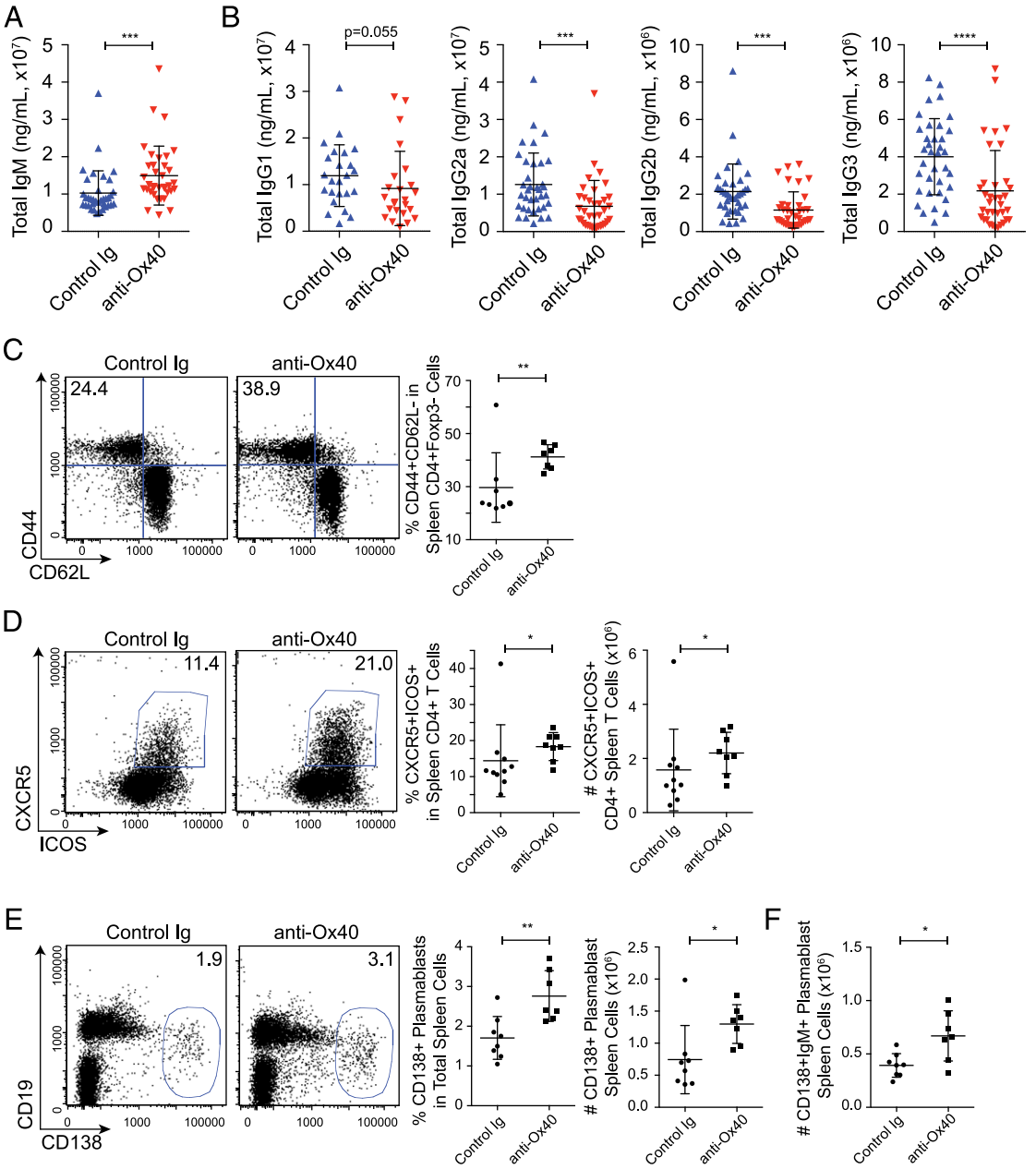

FIGURE 4. Ox40-stimulated splenic T cell response, plasmablast accumulation, and Ig effects. Quantification of total serum IgM concentration (**A**) and total serum IgG1, IgG2a, IgG2b, and IgG3 concentrations (**B**) following anti-Ox40 mAb treatment presented as mean ± SD combined from three independent cohorts (n = 24 for IgG1 and 36 for all other groups, combined). (**C**–**E**) Representative flow cytometry plots (left panels) and summary data (right panels) from NZB/W F1 spleen preparations presented with mean ± SD. (C) Frequency of activation/memory cell markers CD44 and CD62L on Tconv cells (gated live $CD45^+CD3^+CD4^+Foxp3^-$). (D) Frequency and total number of $CXCR5^+ICOS^+$ Tfh cells (gated $CD3^+CD4^+$). (E) Frequency and total number of plasmablast cells ($CD138^+$). (**F**) Total number of IgM^+CD138^+ plasmablast cells. *$p < 0.05$, **$p < 0.01$, ***$p < 0.001$, ****$p < 0.0001$.

Differentially expressed genes were identified by comparing nRPKM between T cells purified from Ox40 agonist mAb–treated and control Ig–treated mice and applying a strict set of statistical criteria: fold change > 2 (or <0.5), p value < 0.05, and mean nRPKM > 2 (see *Materials and Methods*).

Following anti-Ox40 mAb treatment, 186 genes were significantly induced and 6 were repressed in splenic CD4 T cells (Supplemental Fig. 4A). In the kidney, 188 genes were significantly upregulated, and 31 were repressed (Supplemental Fig. 4B). Ninety-three upregulated genes were shared between the spleen and kidney (Fig. 5A, Supplemental Fig. 4C); however, a larger fraction of genes were not shared (60% of splenic T cell transcripts and 51% of the kidney).

Pathway analysis of the shared genes indicated that the most enriched cellular and molecular pathways were cell cycle, cellular assembly, and DNA replication. *Mki67*, a marker for T cell proliferation, was enriched in splenic and kidney CD4 T cells (Supplemental Fig. 4A, 4B). Transcriptional evidence for cycling cells was particularly prominent (Proliferation of Cells, 52 genes, $p = 2.58 \times 10^{-10}$) (Supplemental Fig. 4D). Consistent with the accumulation of Tregs observed by flow cytometry, *foxp3* and other Treg-related functional genes were also upregulated (Supplemental Fig. 4E).

Pathway analysis of the splenic T cell RNASeq data indicated that Interferon Signaling ($p = 2.49 \times 10^{-7}$) genes were strongly upregulated in the Ox40 mAb–stimulated T cells. We confirmed

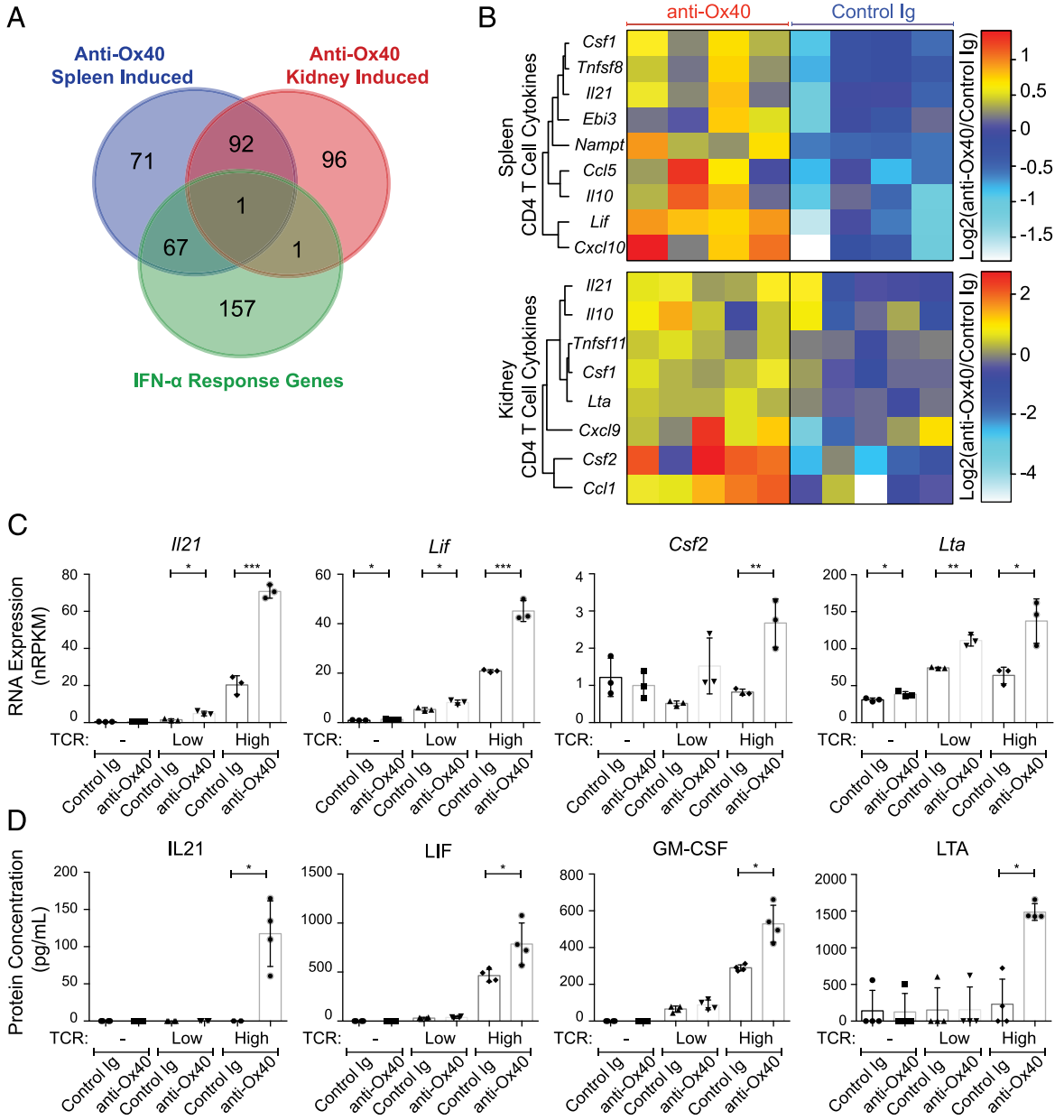

FIGURE 5. Gene expression and cytokine production changes in Ox40-stimulated CD4 T cells. (**A** and **B**) RNA was collected from sorted live CD45$^+$ CD19$^-$CD3$^+$CD4$^+$ T cells from the spleen (n = 4) and kidney (n = 5) of 21–27-wk-old NZB/W F1 mice with 30–100 mg/dl proteinuria (at the start of treatment) after 1 wk (day 8) of anti-Ox40 agonist mAb treatment, followed by RNASeq analysis. (A) Venn diagram showing the overlap of gene-expression changes from anti-Ox40 mAb treatment in the spleen and kidney, with a splenic CD4 T cell IFN-α response gene dataset (43). (B) Heat map euclidean clustering of genes with the cytokine classification (IPA) induced ($p < 0.05$, nRPKM > 2, and fold-change > 1.5) following anti-Ox40 mAb treatment in spleen (upper panel) or kidney (lower panel) CD4 T cells. (**C** and **D**) Cultured CD4 T cells from the spleen of 21–27-wk-old NZB/W F1 mice with 30–100 mg/dl proteinuria (as in the in vivo treatments). Cells were cultured with a 0 (-), 1:10 (Low), or 1:1 (High) ratio of TCR-stimulating anti-CD3/CD28 beads with anti-Ox40 mAb or control Ig treatment for 48 h, followed by RNASeq on the cells and supernatant protein analysis. Cytokine genes were selected based on identification in (B) and protein concentrations were measured for the strongest induced genes (by RNA). RNA expression (nRPKM) (C) and supernatant protein concentration (pg/ml) (D) presented as mean ± SD combined from at least two independent experiments. *$p < 0.05$, **$p < 0.01$, ***$p < 0.001$.

the enrichment for IFN-regulated genes by comparing the Ox40-induced genes with a CD4 T cell IFN-α response gene dataset (43) and found that 29% of induced genes in the spleen (67/231) were IFN-α regulated compared with only 1% (2/190) in the kidney (Fig. 5A). This finding is particularly interesting given the strong evidence for activation of type I IFN–induced genes in human SLE (45).

Pathway analysis also identified enrichment for Quantity of Interleukins (11 genes, $p = 3.03 \times 10^{-8}$), Movement of T Cells (5 genes, $p = 6.44 \times 10^{-7}$), and Recruitment of Leukocytes (13 genes, $p = 1.22 \times 10^{-5}$). These enriched functional pathways included inflammatory cytokines and chemokines, a number of which have been implicated in SLE pathogenesis (46). We broadened our search for genes of the cytokine classification (>1.5-fold change) and found that *Il21*, *Csf1*, and *Il10* were significantly induced in spleen and kidney T cells (Fig. 5B). *Cxcl10*, *Ccl5*, *Ebi3*, *Nampt*, *Tnfsf8*, and *Lif* transcripts were upregulated in spleen T cells, and *Csf2*, *Cxcl9*, *Ccl1*, *Lta*, and *Tnfsf11* were elevated in kidney T cells.

TCR-dependent cytokine production following Ox40 agonist mAb treatment

To further explore the relationship between Ox40-stimulated cytokine production and TCR signaling, we cultured purified CD4 T cells in vitro with anti-Ox40 mAbs in the presence or absence of various levels of TCR stimulation (see *Materials and Methods*). Cells were harvested for RNA, and culture supernatants were collected for cytokine protein quantification.

Of the 14 cytokines identified from the in vivo RNA experiments, four mRNAs (*Il21*, *Lif*, *Csf2*, and *Lta*) showed strong responses in vitro to anti-Ox40 mAb treatment (Fig. 5C, Supplemental Fig. 4F). *Il21*, *Lif*, and *Csf2* were expressed at background levels (<2 nRPKM) in the absence of TCR stimulation, whereas *Lta* was moderately expressed at baseline. TCR stimulation alone induced expression of *Il21*, *Lif*, and *Lta*, and higher expression levels were observed for all four cytokine transcripts following combined TCR and anti-Ox40 mAb stimulation.

We next measured supernatant protein for the most highly induced genes and found that TCR stimulation was required for detectable IL-21, LIF, GM-CSF (*Csf2*), and LTA production (Fig. 5D). LIF and GM-CSF were induced with high TCR alone and were further increased by concomitant anti-Ox40 mAb treatment. IL-21 and LTA production required a combination of high TCR and anti-Ox40 mAb treatment. From these data, we conclude that Ox40-induced inflammatory cytokine production in this in vitro system was dependent on TCR stimulation.

Ox40L blockade delays worsening of renal disease and death

Finally, we tested whether blockade of Ox40/Ox40L interactions would have a therapeutic effect in the IFN-α–accelerated NZB/W F1 lupus model. We used this model, rather than the spontaneous NZB/W F1 model, because it may more accurately model the disease of human SLE patients, who often have prominent type I IFN signatures in blood and tissues (45). The IFN-accelerated model has an added benefit of synchronizing and shortening the normally variable disease course found in NZB/W F1 mice (47). However, the disease found in these animals is more aggressive and resistant to therapy (48). We used a soluble Ox40:Fc fusion protein to block Ox40L (see *Materials and Methods*) and treated 12-wk-old proteinuria-free mice twice a week for the duration of the 15-wk experiment. The initial dose of Ox40:Fc was given 3 d after injection with an IFN-α–expressing adenoviral vector. Across two independent cohorts, Ox40:Fc treatment resulted in a delay in the onset of severe renal disease (≥300 mg/dl proteinuria, median onset = 40 d) compared with control treatment (median onset = 27 d, hazard ratio = 0.5, $p < 0.006$) (Fig. 6A).

Ox40:Fc extended the lifespan of treated animals by ∼2 wk (Fig. 6B). The median survival was extended from day 55 in the control group to day 70 in the Ox40:Fc group (hazard ratio = 0.48, $p < 0.008$). These data provide the first in vivo evidence, to our knowledge, that the Ox40/Ox40L pathway has a role in mediating renal disease in a lupus model.

Discussion

Despite the strong genetic evidence that variants in the Ox40L locus contribute to human SLE risk, there are still significant gaps in our understanding of this pathway's role in SLE pathogenesis. In the current study, we demonstrate that Ox40-expressing T cells (including follicular, regulatory, and conventional helper subsets) were present in spleens and kidneys of NZB/W F1 lupus-prone mice and increased during progressive disease; in vivo agonism of the Ox40/Ox40L pathway, using an anti-Ox40 mAb, potently exacerbated renal disease; Ox40 stimulation induced kidney-infiltrating and splenic CD4 T cell activation, splenic Tfh cell and plasmablast accumulation, serum IgM elevation, and kidney IgM deposition; Ox40 signaling induced an inflammatory and proliferative transcriptional program in CD4 T cells, including a prominent upregulation of type I IFN–induced genes in the spleen; Ox40 stimulation also led to elevated production of TCR-dependent inflammatory cytokines, including IL-21; and in vivo blockade of Ox40/Ox40L signaling using an Fc-fusion protein showed significant benefit on disease progression and death in an IFN-α–accelerated NZB/W F1 model.

Based on these findings, we conclude that the Ox40/Ox40L pathway contributes to lupus pathogenesis by promoting several specific Th cell functions, such as controlling Tfh cell accumulation and cytokine production in lymphoid tissues and increasing the number of presumably pathogenic Ab-producing plasmablasts. Ox40 stimulation also led to significant worsening of renal disease that was mediated, at least in part, by deposition of IgM in glomeruli and production of inflammatory cytokines and chemokines by T cells residing in the kidney. These data provide new insights into the mechanisms by which Ox40/Ox40L interactions can contribute to systemic and tissue autoimmunity, as well as provide experimental evidence that blockade of this pathway may provide therapeutic benefit in lupus.

Recently, Jacquemin et al. (49) demonstrated that Ox40 stimulation of human T cells in vitro promoted a Tfh cell-like transcriptional program and phenotype. They also described an Ox40L-expressing myeloid APC population in SLE patient blood and kidney tissue, with the frequency of Ox40L-expressing cells correlating with numbers of blood Tfh cells and disease

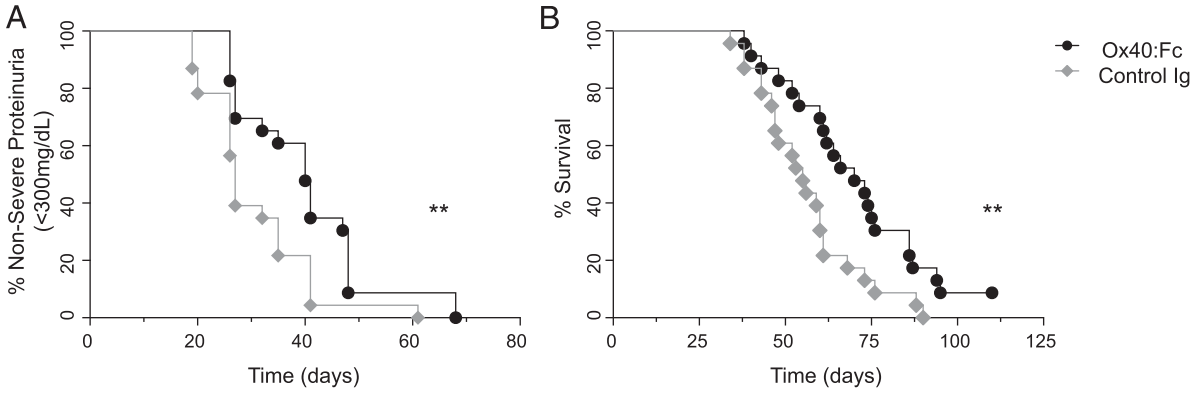

FIGURE 6. Blocking Ox40L results in delayed IFN-α–accelerated renal disease and death. Renal disease (**A**) and survival (**B**) following Ox40:Fc or control Ig treatment (20 mg/kg, twice weekly, for the duration of the experiment) in Ad5–IFN-α vector–accelerated 12-wk-old proteinuria-free NZB/W F1 mice (two independent cohorts combined, $n = 23$). $^{**}p < 0.01$.

activity. The increased numbers of Tfh cells and the cytokine production that we identified following in vivo anti-Ox40 mAb treatment are consistent with the hypothesis that Ox40 signaling promotes Tfh cell accumulation and function. Tfh cells provide several forms of B cell help (20, 21), but the precise disease-relevant contribution from Ox40 has not been well described for lupus.

We propose that the accumulation of plasmablasts, including IgM^+ cells, increased serum IgM levels, decreased IgG levels, and the absence of a change in GCs or GC cell numbers, suggests that Ox40 may stimulate Th cells, resulting in extrafollicular or pre-GC reactions. A similar role has been ascribed for the costimulatory molecule ICOS (50). Ox40 stimulation may promote B cells that might otherwise enter a GC to differentiate into plasmablasts. A recent publication describing Ox40/Ox40L interactions located inside and outside of GCs during infection supports this possibility (32); however, in that study, Ox40 was required for GC formation and anti-viral Ab responses, highlighting the disease-specific nature of this pathway. On the whole, our data support the hypothesis that the Ox40/Ox40L pathway promotes lupus pathogenesis by regulating plasmablast accumulation and serum IgM levels, rather than promoting GCs or class switching.

Ox40-mediated upregulation of IL-21 may be important for the amplified IgM response, given that IL-21 can enhance the generation of IgM-expressing memory B cells, IgM-expressing plasma cells, and production of soluble IgM (51–55). Disruption of the IL-21 pathway has provided benefit in several preclinical lupus models. These studies have included full genetic deletion or B cell–specific deletion of IL-21R in the BXSB-Yaa model (56, 57), IL-21R–Fc treatment in the MRL-Fas^{Lpr} model (58), anti–IL-21R mAb treatment in the NZB/W F1 model (59), and anti–IL-21 mAb treatment in the B6.*Sle.Yaa* model (60).

Human genetics evidence further connects the Ox40/Ox40L pathway with Ab responses in the setting of autoimmunity. One of the Ox40L locus polymorphisms associated with SLE risk (rs2205960-T) showed significant correlation with serum autoantibody titers in lupus cases from diverse ancestry (61). Ox40L locus polymorphisms have been associated with systemic sclerosis (62, 63) and, in particular, autoantibody-associated cases (64), as well as Sjögren's syndrome (65), a disease characterized by autoantibodies. Although Ox40L has not been reported to confer risk for rheumatoid arthritis, one study identified an association between serum Ox40L protein levels and anti-citrullinated protein Abs, as well as IgM rheumatoid factor, in rheumatoid arthritis patients (66).

Stimulation of Ox40 using agonist mAbs was surprisingly potent and resulted in exacerbated renal disease in NZB/W F1 mice with mild-to-moderate pre-existing proteinuria, but not in younger proteinuria-free animals, despite their harboring of Ox40-expressing T cells. This finding suggests that the number or type of Ox40-expressing cells in the spleen or kidney, or the per-cell amount of Ox40, may be important in this system for disease acceleration. Notably, our findings share similarities with other studies using Ox40 agonist treatments. Ox40 agonist treatment exacerbated models of experimental uveitis (67, 68) and promoted inflammatory lung pathology in B6 mice (69). However, in other models, the disease-promoting effects of Ox40 agonism depended upon age and disease severity of the animals (e.g., in experimental autoimmune encephalitis and type 1 diabetes, in which treatment promoted disease during later or effector phases but protected from disease when provided during early or priming phases) (70–72). Evidence from those studies suggests that the disease-promoting versus disease-preventing effects of Ox40 agonism might be explained by how each treatment impacted Tregs in these models. In agreement, coprovision of Treg-boosting treatments, such as IL-2 or JAG1, could reverse the pathogenic effects of Ox40 agonist treatment (69, 73).

We observed an accumulation of $Foxp3^+$ Tregs following anti-Ox40 mAb treatment, despite the progression of autoimmunity. These findings are in line with previous reports of Tregs in aged NZB/W F1 mice, which retain functional regulatory capacity but are unable to control disease (74, 75). Treg-enriched RNA transcripts (*Foxp3*, *Il2ra*, *Itgae*, *Lrrc32*, *Pdcd1*, *Tigit*, and *Tgfb*) were also upregulated by anti-Ox40 mAb treatment, suggesting functional potential. Although we do not have definitive data explaining why these Tregs do not suppress the pathogenic response, there are several possibilities: the regulatory and effector cells are not in the same anatomical location, the expanded Tregs are not relevant for the specific response, or most likely, the activating effect of the Ox40 agonist mAbs on effector T cells overwhelms the suppressive ability of Tregs.

The transcriptional response in purified T cells following in vivo Ox40 agonism included an IFN signature in the spleens of NZB/W F1 mice; nearly one third of the induced splenic transcripts overlapped with genes induced by IFN-α in CD4 T cells (43). The nature of the splenic IFN response is unclear; however, we suspect that it is indirect (i.e., requiring other cells, likely myeloid cells), because anti-Ox40 mAb–stimulated monocellular in vitro cultures did not result in the same IFN signature. An important future direction for this work will be to understand the chain of events by which Ox40 stimulation leads to a type I IFN response, because the IFN signature is prominent in SLE patients (45).

Ox40-stimulating mAbs are currently in early-stage clinical trials for a variety of human cancers (76, 77). Our results suggest the possibility that stimulation of Ox40 in humans may result in untoward autoimmune or inflammatory responses, particularly for individuals with clinical or subclinical autoimmunity. These data also suggest that targeting the Ox40/Ox40L pathway may result in clinical benefit for SLE and/or LN patients. Although our treatment regimen only resulted in a delay (as opposed to complete prevention) in renal disease and death, the model we used has been demonstrated to be particularly aggressive and resistant to therapeutic intervention (47, 48). It remains possible that Ox40- or Ox40L-blocking therapies would show greater efficacy in a spontaneous disease model. Additional studies are needed to fully understand the pathologic consequences of modulating the Ox40/Ox40L pathway, including determining when and how it can be targeted safely and effectively in cancer and autoimmunity.

Acknowledgments

We thank Michael Townsend and Andrey Shaw for manuscript feedback; Phil Hass and Ryan Abraham for production of the Ox40:Fc fusion protein; Jovencio Borneo, Terence Ho, Jonathan Paw, and C.K. Poon for cell sorting; Andres Paler Martinez for Luminex; Xiumin Wu, Juan Zhang, and John Liu for assistance with mouse experiments; Debra Dunlap, Felix Chu, and Sreedevi Chalasani for IHC and immunofluorescence; Charles Havnar, Sarajane Saturnio, and Carmina Espiritu for histology; Zora Modrusan and Jeremy Stinson for assistance with RNASeq; and Jennifer Tom and Bill Forrest for statistical advice. We also thank Cara Skon, Nandhini Ramamoorthi, and the rest of the Human Genetics and Diagnostic Discovery departments for scientific discussion.

Disclosures

All of the authors are full-time employees of Genentech, Inc.

References

1. Davidson, A. 2016. What is damaging the kidney in lupus nephritis? *Nat. Rev. Rheumatol.* 12: 143–153.
2. Liu, Z., and A. Davidson. 2012. Taming lupus-a new understanding of pathogenesis is leading to clinical advances. *Nat. Med.* 18: 871–882.
3. Mannik, M., C. E. Merrill, L. D. Stamps, and M. H. Wener. 2003. Multiple autoantibodies form the glomerular immune deposits in patients with systemic lupus erythematosus. *J. Rheumatol.* 30: 1495–1504.

4. Rahman, A., and D. A. Isenberg. 2008. Systemic lupus erythematosus. *N. Engl. J. Med.* 358: 929–939.
5. Tsokos, G. C. 2011. Systemic lupus erythematosus. *N. Engl. J. Med.* 365: 2110–2121.
6. Bentham, J., D. L. Morris, D. S. Cunninghame Graham, C. L. Pinder, P. Tombleson, T. W. Behrens, J. Martín, B. P. Fairfax, J. C. Knight, L. Chen, et al. 2015. Genetic association analyses implicate aberrant regulation of innate and adaptive immunity genes in the pathogenesis of systemic lupus erythematosus. *Nat. Genet.* 47: 1457–1464.
7. Cunninghame Graham, D. S., R. R. Graham, H. Manku, A. K. Wong, J. C. Whittaker, P. M. Gaffney, K. L. Moser, J. D. Rioux, D. Altshuler, T. W. Behrens, and T. J. Vyse. 2008. Polymorphism at the TNF superfamily gene TNFSF4 confers susceptibility to systemic lupus erythematosus. *Nat. Genet.* 40: 83–89.
8. Croft, M., T. So, W. Duan, and P. Soroosh. 2009. The significance of OX40 and OX40L to T-cell biology and immune disease. *Immunol. Rev.* 229: 173–191.
9. Croft, M. 2010. Control of immunity by the TNFR-related molecule OX40 (CD134). *Annu. Rev. Immunol.* 28: 57–78.
10. Ishii, N., T. Takahashi, P. Soroosh, and K. Sugamura. 2010. OX40-OX40 ligand interaction in T-cell-mediated immunity and immunopathology. *Adv. Immunol.* 105: 63–98.
11. Webb, G. J., G. M. Hirschfield, and P. J. Lane. 2016. OX40, OX40L and autoimmunity: a comprehensive review. *Clin. Rev. Allergy Immunol.* 50: 312–332.
12. Rogers, P. R., J. Song, I. Gramaglia, N. Killeen, and M. Croft. 2001. OX40 promotes Bcl-xL and Bcl-2 expression and is essential for long-term survival of CD4 T cells. *Immunity* 15: 445–455.
13. Song, J., S. Salek-Ardakani, P. R. Rogers, M. Cheng, L. Van Parijs, and M. Croft. 2004. The costimulation-regulated duration of PKB activation controls T cell longevity. *Nat. Immunol.* 5: 150–158.
14. Song, J., T. So, M. Cheng, X. Tang, and M. Croft. 2005. Sustained survivin expression from OX40 costimulatory signals drives T cell clonal expansion. *Immunity* 22: 621–631.
15. Gramaglia, I., A. D. Weinberg, M. Lemon, and M. Croft. 1998. Ox-40 ligand: a potent costimulatory molecule for sustaining primary CD4 T cell responses. *J. Immunol.* 161: 6510–6517.
16. Gramaglia, I., A. Jember, S. D. Pippig, A. D. Weinberg, N. Killeen, and M. Croft. 2000. The OX40 costimulatory receptor determines the development of CD4 memory by regulating primary clonal expansion. *J. Immunol.* 165: 3043–3050.
17. Murata, K., N. Ishii, H. Takano, S. Miura, L. C. Ndhlovu, M. Nose, T. Noda, and K. Sugamura. 2000. Impairment of antigen-presenting cell function in mice lacking expression of OX40 ligand. *J. Exp. Med.* 191: 365–374.
18. Takeda, I., S. Ine, N. Killeen, L. C. Ndhlovu, K. Murata, S. Satomi, K. Sugamura, and N. Ishii. 2004. Distinct roles for the OX40-OX40 ligand interaction in regulatory and nonregulatory T cells. *J. Immunol.* 172: 3580–3589.
19. Valzasina, B., C. Guiducci, H. Dislich, N. Killeen, A. D. Weinberg, and M. P. Colombo. 2005. Triggering of OX40 (CD134) on CD4(+)CD25+ T cells blocks their inhibitory activity: a novel regulatory role for OX40 and its comparison with GITR. *Blood* 105: 2845–2851.
20. Ueno, H., J. Banchereau, and C. G. Vinuesa. 2015. Pathophysiology of T follicular helper cells in humans and mice. *Nat. Immunol.* 16: 142–152.
21. Crotty, S. 2014. T follicular helper cell differentiation, function, and roles in disease. *Immunity* 41: 529–542.
22. Blanco, P., H. Ueno, and N. Schmitt. 2016. T follicular helper (Tfh) cells in lupus: activation and involvement in SLE pathogenesis. *Eur. J. Immunol.* 46: 281–290.
23. Vinuesa, C. G., M. C. Cook, C. Angelucci, V. Athanasopoulos, L. Rui, K. M. Hill, D. Yu, H. Domaschenz, B. Whittle, T. Lambe, et al. 2005. A RING-type ubiquitin ligase family member required to repress follicular helper T cells and autoimmunity. *Nature* 435: 452–458.
24. Yu, D., A. H. Tan, X. Hu, V. Athanasopoulos, N. Simpson, D. G. Silva, A. Hutloff, K. M. Giles, P. J. Leedman, K. P. Lam, et al. 2007. Roquin represses autoimmunity by limiting inducible T-cell co-stimulator messenger RNA. *Nature* 450: 299–303.
25. Linterman, M. A., R. J. Rigby, R. K. Wong, D. Yu, R. Brink, J. L. Cannons, P. L. Schwartzberg, M. C. Cook, G. D. Walters, and C. G. Vinuesa. 2009. Follicular helper T cells are required for systemic autoimmunity. *J. Exp. Med.* 206: 561–576.
26. Vogel, K. U., S. L. Edelmann, K. M. Jeltsch, A. Bertossi, K. Heger, G. A. Heinz, J. Zöller, S. C. Warth, K. P. Hoefig, C. Lohs, et al. 2013. Roquin paralogs 1 and 2 redundantly repress the Icos and Ox40 costimulator mRNAs and control follicular helper T cell differentiation. *Immunity* 38: 655–668.
27. Stüber, E., and W. Strober. 1996. The T cell-B cell interaction via OX40-OX40L is necessary for the T cell-dependent humoral immune response. *J. Exp. Med.* 183: 979–989.
28. Kopf, M., C. Ruedl, N. Schmitz, A. Gallimore, K. Lefrang, B. Ecabert, B. Odermatt, and M. F. Bachmann. 1999. OX40-deficient mice are defective in Th cell proliferation but are competent in generating B cell and CTL responses after virus infection. *Immunity* 11: 699–708.
29. Chen, A. I., A. J. McAdam, J. E. Buhlmann, S. Scott, M. L. Lupher, Jr., E. A. Greenfield, P. R. Baum, W. C. Fanslow, D. M. Calderhead, G. J. Freeman, and A. H. Sharpe. 1999. Ox40-ligand has a critical costimulatory role in dendritic cell:T cell interactions. *Immunity* 11: 689–698.
30. Pippig, S. D., C. Peña-Rossi, J. Long, W. R. Godfrey, D. J. Fowell, S. L. Reiner, M. L. Birkeland, R. M. Locksley, A. N. Barclay, and N. Killeen. 1999. Robust B cell immunity but impaired T cell proliferation in the absence of CD134 (OX40). *J. Immunol.* 163: 6520–6529.
31. Boettler, T., F. Moeckel, Y. Cheng, M. Heeg, S. Salek-Ardakani, S. Crotty, M. Croft, and M. G. von Herrath. 2012. OX40 facilitates control of a persistent virus infection. *PLoS Pathog.* 8: e1002913.
32. Tahiliani, V., T. E. Hutchinson, G. Abboud, M. Croft, and S. Salek-Ardakani. 2017. OX40 cooperates with ICOS to amplify follicular Th cell development and germinal center reactions during infection. *J. Immunol.* 198: 218–228.
33. Brocker, T., A. Gulbranson-Judge, S. Flynn, M. Riedinger, C. Raykundalia, and P. Lane. 1999. CD4 T cell traffic control: in vivo evidence that ligation of OX40 on CD4 T cells by OX40-ligand expressed on dendritic cells leads to the accumulation of CD4 T cells in B follicles. *Eur. J. Immunol.* 29: 1610–1616.
34. Flynn, S., K. M. Toellner, C. Raykundalia, M. Goodall, and P. Lane. 1998. CD4 T cell cytokine differentiation: the B cell activation molecule, OX40 ligand, instructs CD4 T cells to express interleukin 4 and upregulates expression of the chemokine receptor, Blr-1. *J. Exp. Med.* 188: 297–304.
35. Walker, L. S., A. Gulbranson-Judge, S. Flynn, T. Brocker, C. Raykundalia, M. Goodall, R. Förster, M. Lipp, and P. Lane. 1999. Compromised OX40 function in CD28-deficient mice is linked with failure to develop CXC chemokine receptor 5-positive CD4 cells and germinal centers. *J. Exp. Med.* 190: 1115–1122.
36. Kim, M.-Y., F. M. Gaspal, H. E. Wiggett, F. M. McConnell, A. Gulbranson-Judge, C. Raykundalia, L. S. Walker, M. D. Goodall, and P. J. Lane. 2003. CD4(+)CD3(-) accessory cells costimulate primed CD4 T cells through OX40 and CD30 at sites where T cells collaborate with B cells. *Immunity* 18: 643–654.
37. Zhou, Y.-B., R.-G. Ye, Y.-J. Li, C.-M. Xie, and Y.-H. Wu. 2008. Effect of anti-CD134L mAb and CTLA4Ig on ConA-induced proliferation, Th cytokine secretion, and anti-dsDNA antibody production in spleen cells from lupus-prone BXSB mice. *Autoimmunity* 41: 395–404.
38. Zhou, Y.-B., R.-G. Ye, Y.-J. Li, and C.-M. Xie. 2009. Targeting the CD134-CD134L interaction using anti-CD134 and/or rhCD134 fusion protein as a possible strategy to prevent lupus nephritis. *Rheumatol. Int.* 29: 417–425.
39. Perry, D., A. Sang, Y. Yin, Y.-Y. Zheng, and L. Morel. 2011. Murine models of systemic lupus erythematosus. *J. Biomed. Biotechnol.* 2011: 271694.
40. Srinivasan, K., B. A. Friedman, J. L. Larson, B. E. Lauffer, L. D. Goldstein, L. L. Appling, J. Borneo, C. Poon, T. Ho, F. Cai, et al. 2016. Untangling the brain's neuroinflammatory and neurodegenerative transcriptional responses. *Nat. Commun.* 7: 11295.
41. Wu, T. D., J. Reeder, M. Lawrence, G. Becker, and M. J. Brauer. 2016. GMAP and GSNAP for genomic sequence alignment: enhancements to speed, accuracy, and functionality. *Methods Mol. Biol.* 1418: 283–334.
42. Law, C. W., Y. Chen, W. Shi, and G. K. Smyth. 2014. Voom: precision weights unlock linear model analysis tools for RNA-seq read counts. *Genome Biol.* 15: R29.
43. Mostafavi, S., H. Yoshida, D. Moodley, H. LeBoité, K. Rothamel, T. Raj, C. J. Ye, N. Chevrier, S.-Y. Zhang, T. Feng, et al; Immunological Genome Project Consortium. 2016. Parsing the interferon transcriptional network and its disease associations. *Cell* 164: 564–578.
44. Crotty, S. 2011. Follicular helper CD4 T cells (TFH). *Annu. Rev. Immunol.* 29: 621–663.
45. Baechler, E. C., F. M. Batliwalla, G. Karypis, P. M. Gaffney, W. A. Ortmann, K. J. Espe, K. B. Shark, W. J. Grande, K. M. Hughes, V. Kapur, et al. 2003. Interferon-inducible gene expression signature in peripheral blood cells of patients with severe lupus. *Proc. Natl. Acad. Sci. USA* 100: 2610–2615.
46. Nowling, T. K., and G. S. Gilkeson. 2011. Mechanisms of tissue injury in lupus nephritis. *Arthritis Res. Ther.* 13: 250.
47. Liu, Z., and A. Davidson. 2013. IFNα inducible models of murine SLE. *Front. Immunol.* 4: 306.
48. Liu, Z., R. Bethunaickan, W. Huang, M. Ramanujam, M. P. Madaio, and A. Davidson. 2011. IFN-α confers resistance of systemic lupus erythematosus nephritis to therapy in NZB/W F1 mice. *J. Immunol.* 187: 1506–1513.
49. Jacquemin, C., N. Schmitt, C. Contin-Bordes, Y. Liu, P. Narayanan, J. Seneschal, T. Maurouard, D. Dougall, E. S. Davizon, H. Dumortier, et al. 2015. OX40 ligand contributes to human lupus pathogenesis by promoting T follicular helper response. *Immunity* 42: 1159–1170.
50. Odegard, J. M., B. R. Marks, L. D. DiPlacido, A. C. Poholek, D. H. Kono, C. Dong, R. A. Flavell, and J. Craft. 2008. ICOS-dependent extrafollicular helper T cells elicit IgG production via IL-21 in systemic autoimmunity. *J. Exp. Med.* 205: 2873–2886.
51. Ozaki, K., R. Spolski, R. Ettinger, H.-P. Kim, G. Wang, C.-F. Qi, P. Hwu, D. J. Shaffer, S. Akilesh, D. C. Roopenian, et al. 2004. Regulation of B cell differentiation and plasma cell generation by IL-21, a novel inducer of Blimp-1 and Bcl-6. *J. Immunol.* 173: 5361–5371.
52. Good, K. L., V. L. Bryant, and S. G. Tangye. 2006. Kinetics of human B cell behavior and amplification of proliferative responses following stimulation with IL-21. *J. Immunol.* 177: 5236–5247.
53. Ettinger, R., G. P. Sims, A.-M. Fairhurst, R. Robbins, Y. S. da Silva, R. Spolski, W. J. Leonard, and P. E. Lipsky. 2005. IL-21 induces differentiation of human naive and memory B cells into antibody-secreting plasma cells. *J. Immunol.* 175: 7867–7879.
54. Bryant, V. L., C. S. Ma, D. T. Avery, Y. Li, K. L. Good, L. M. Corcoran, R. de Waal Malefyt, and S. G. Tangye. 2007. Cytokine-mediated regulation of human B cell differentiation into Ig-secreting cells: predominant role of IL-21 produced by CXCR5+ T follicular helper cells. *J. Immunol.* 179: 8180–8190.
55. Avery, D. T., E. K. Deenick, C. S. Ma, S. Suryani, N. Simpson, G. Y. Chew, T. D. Chan, U. Palendira, J. Bustamante, S. Boisson-Dupuis, et al. 2010. B cell-intrinsic signaling through IL-21 receptor and STAT3 is required for establishing long-lived antibody responses in humans. *J. Exp. Med.* 207: 155–171.
56. Bubier, J. A., T. J. Sproule, O. Foreman, R. Spolski, D. J. Shaffer, H. C. Morse, III, W. J. Leonard, and D. C. Roopenian. 2009. A critical role for IL-21 receptor signaling in the pathogenesis of systemic lupus erythematosus in BXSB-Yaa mice. *Proc. Natl. Acad. Sci. USA* 106: 1518–1523.

57. McPhee, C. G., J. A. Bubier, T. J. Sproule, G. Park, M. P. Steinbuck, W. H. Schott, G. J. Christianson, H. C. Morse, III, and D. C. Roopenian. 2013. IL-21 is a double-edged sword in the systemic lupus erythematosus-like disease of BXSB.Yaa mice. *J. Immunol.* 191: 4581–4588.
58. Herber, D., T. P. Brown, S. Liang, D. A. Young, M. Collins, and K. Dunussi-Joannopoulos. 2007. IL-21 has a pathogenic role in a lupus-prone mouse model and its blockade with IL-21R.Fc reduces disease progression. *J. Immunol.* 178: 3822–3830.
59. Zhang, M., G. Yu, B. Chan, J. T. Pearson, P. Rathanaswami, J. Delaney, A. Ching Lim, J. Babcook, H. Hsu, and M. A. Gavin. 2015. Interleukin-21 receptor blockade inhibits secondary humoral responses and halts the progression of preestablished disease in the (NZB × NZW)F1 systemic lupus erythematosus model. *Arthritis Rheumatol.* 67: 2723–2731.
60. Choi, J.-Y., A. Seth, M. Kashgarian, S. Terrillon, E. Fung, L. Huang, L. C. Wang, and J. Craft. 2017. Disruption of pathogenic cellular networks by IL-21 blockade leads to disease amelioration in murine lupus. *J. Immunol.* 198: 2578–2588.
61. Manku, H., C. D. Langefeld, S. G. Guerra, T. H. Malik, M. Alarcon-Riquelme, J.-M. Anaya, S.-C. Bae, S. A. Boackle, E. E. Brown, L. A. Criswell, et al. 2013. Trans-ancestral studies fine map the SLE-susceptibility locus TNFSF4. *PLoS Genet.* 9: e1003554.
62. Gourh, P., F. C. Arnett, F. K. Tan, S. Assassi, D. Divecha, G. Paz, T. McNearney, H. Draeger, J. D. Reveille, M. D. Mayes, and S. K. Agarwal. 2010. Association of TNFSF4 (OX40L) polymorphisms with susceptibility to systemic sclerosis. *Ann. Rheum. Dis.* 69: 550–555.
63. Bossini-Castillo, L., J. C. Broen, C. P. Simeon, L. Beretta, M. C. Vonk, N. Ortego-Centeno, G. Espinosa, P. Carreira, M. T. Camps, N. Navarrete, et al. 2011. A replication study confirms the association of TNFSF4 (OX40L) polymorphisms with systemic sclerosis in a large European cohort. *Ann. Rheum. Dis.* 70: 638–641.
64. Coustet, B., M. Bouaziz, P. Dieudé, M. Guedj, L. Bossini-Castillo, S. Agarwal, T. Radstake, J. Martin, P. Gourh, M. Elhai, et al. 2012. Independent replication and meta analysis of association studies establish TNFSF4 as a susceptibility gene preferentially associated with the subset of anticentromere-positive patients with systemic sclerosis. *J. Rheumatol.* 39: 997–1003.
65. Nordmark, G., G. Kristjansdottir, E. Theander, S. Appel, P. Eriksson, L. Vasaitis, M. Kvarnström, N. Delaleu, P. Lundmark, A. Lundmark, et al. 2011. Association of EBF1, FAM167A(C8orf13)-BLK and TNFSF4 gene variants with primary Sjögren's syndrome. *Genes Immun.* 12: 100–109.
66. Laustsen, J. K., T. K. Rasmussen, K. Stengaard-Pedersen, K. Hørslev-Petersen, M. L. Hetland, M. Østergaard, P. Junker, M. Hvid, and B. Deleuran. 2014. Soluble OX40L is associated with presence of autoantibodies in early rheumatoid arthritis. *Arthritis Res. Ther.* 16: 474.
67. Zhang, Z., W. Zhong, D. Hinrichs, X. Wu, A. Weinberg, M. Hall, D. Spencer, K. Wegmann, and J. T. Rosenbaum. 2010. Activation of OX40 augments Th17 cytokine expression and antigen-specific uveitis. *Am. J. Pathol.* 177: 2912–2920.
68. Wu, X., J. T. Rosenbaum, G. Adamus, G. L. Zhang, J. Duan, A. Weinberg, and Z. Zhang. 2011. Activation of OX40 prolongs and exacerbates autoimmune experimental uveitis. *Invest. Ophthalmol. Vis. Sci.* 52: 8520–8526.
69. Xiao, X., W. Gong, G. Demirci, W. Liu, S. Spoerl, X. Chu, D. K. Bishop, L. A. Turka, and X. C. Li. 2012. New insights on OX40 in the control of T cell immunity and immune tolerance in vivo. *J. Immunol.* 188: 892–901.
70. Ruby, C. E., M. A. Yates, D. Hirschhorn-Cymerman, P. Chlebeck, J. D. Wolchok, A. N. Houghton, H. Offner, and A. D. Weinberg. 2009. Cutting edge: OX40 agonists can drive regulatory T cell expansion if the cytokine milieu is right. *J. Immunol.* 183: 4853–4857.
71. Bresson, D., G. Fousteri, Y. Manenkova, M. Croft, and M. von Herrath. 2011. Antigen-specific prevention of type 1 diabetes in NOD mice is ameliorated by OX40 agonist treatment. *J. Autoimmun.* 37: 342–351.
72. Haddad, C. S., P. Bhattacharya, K. Alharshawi, A. Marinelarena, P. Kumar, O. El-Sayed, H. A. Elshabrawy, A. L. Epstein, and B. S. Prabhakar. 2016. Age-dependent divergent effects of OX40L treatment on the development of diabetes in NOD mice. *Autoimmunity* 49: 298–311.
73. Kumar, P., K. Alharshawi, P. Bhattacharya, A. Marinelarena, C. Haddad, Z. Sun, S. Chiba, A. L. Epstein, and B. S. Prabhakar. 2017. Soluble OX40L and JAG1 induce selective proliferation of functional regulatory T-cells independent of canonical TCR signaling. *Sci. Rep.* 7: 39751.
74. Iikuni, N., E. V. Lourenço, B. H. Hahn, and A. La Cava. 2009. Cutting edge: regulatory T cells directly suppress B cells in systemic lupus erythematosus. *J. Immunol.* 183: 1518–1522.
75. Abe, J., S. Ueha, J. Suzuki, Y. Tokano, K. Matsushima, and S. Ishikawa. 2008. Increased Foxp3(+) CD4(+) regulatory T cells with intact suppressive activity but altered cellular localization in murine lupus. *Am. J. Pathol.* 173: 1682–1692.
76. Linch, S. N., M. J. McNamara, and W. L. Redmond. 2015. OX40 agonists and combination immunotherapy: putting the pedal to the metal. *Front. Oncol.* 5: 34.
77. Weinberg, A. D., N. P. Morris, M. Kovacsovics-Bankowski, W. J. Urba, and B. D. Curti. 2011. Science gone translational: the OX40 agonist story. *Immunol. Rev.* 244: 218–231.